JOURNAL OF GEOPHYSICAL RESEARCH, VOL. 112, C05026, doi:10.1029/2006JC003843, 2007

Importance of the polarization in the retrieval of oceanic constituents from the remote sensing reflectance

Malik Chami[1]

Received 27 July 2006; revised 20 December 2006; accepted 19 March 2007; published 16 May 2007.

[1] The influence of marine particles on the polarized radiation exiting the ocean is studied, and the implications for the retrieval of particulate concentration from remotely sensed data are investigated. Simulations were carried out using a vector radiative transfer model. Open ocean and coastal waters conditions were examined separately. In phytoplankton dominated waters, the polarized reflectance is virtually insensitive to the variations in chlorophyll concentration when observing at the top of atmosphere. The polarization effects induced by phytoplankton cells are too weak compared to those induced by the air-water interface and the atmospheric particles (especially molecules) to significantly contribute to the polarized reflectance at this level of atmosphere. The use of the polarized information at short wavelengths is thus proposed to improve the retrieval of the spectral variation of the aerosol model in atmospheric correction algorithms. In coastal zones, the sensitivity of the polarized signal to the water content is much greater. The analysis demonstrates that the measurement of the polarized reflectance just above the sea surface may not be relevant to reduce the skylight reflection effects when the water mass is mainly dominated by highly refractive particles. It is shown that polarization measurements can be of great interest to separate the fraction of inorganic particles from biogenic cells. This study also highlights that an empirical-based inversion approach relying on the polarized reflectance measured in the green and at longer wavelengths could be efficient to retrieve the concentration of inorganic particles regardless of the phytoplankton content in coastal waters.

Citation: Chami, M. (2007), Importance of the polarization in the retrieval of oceanic constituents from the remote sensing reflectance, *J. Geophys. Res.*, *112*, C05026, doi:10.1029/2006JC003843.

1. Introduction

[2] The solar incident light interacts with all the components of the atmosphere-ocean system. Each phenomenon of scattering by molecules, aerosols, hydrosols and reflection over the sea surface introduces and modifies the polarization state of light. Therefore, the reflected solar radiation is polarized and contains embedded information about the intrinsic nature of aerosols and suspended matter in the ocean. Most of the detailed physical information (i.e., size distribution, composition) about the particles present in the atmosphere-ocean system is available through the measurement and analysis of the spectral and angular polarization signature of the oceanic and atmospheric radiation. The principal reason for the greater effectiveness of remote sensing by means of polarization measurements is the significantly higher sensitivity of polarization features to particles size, shape and refractive index as a function of scattering angle and wavelength, than is the case for intensity measurements. The strength of polarization features has been widely demonstrated in the case of aerosol retrievals [*Goloub et al.*, 1999; *Chowdhary et al.*, 2002; *Li et al.*, 2006]. However, retrievals of subsurface particulate matter properties using polarization and remotely sensed data has not been extensively studied yet. This is mainly because of practical difficulties in achieving reliable *in-situ* measurements. Most of the available observations were carried out decades ago [*Waterman*, 1954, 1955; *Ivanoff and Waterman*, 1958; *Beardsley*, 1968; *Lundgren and Hojerslev*, 1971; *Voss and Fry*, 1984]. Another factor that contributes to reduce the number of studies about oceanic polarization is that most current methods of radiative transfer treat light as a scalar. As an example, the commonly used Hydrolight, CDISORT or Morel and Gentili's [1996] Monte Carlo radiative transfer models do not account for the polarization of the oceanic radiation.

[3] Based on a radiative transfer model (so-called OSOA model) that was developed to predict the radiance and the degree of polarization in the coupled ocean-atmosphere system, *Chami et al.* [2001] studied the polarizing properties of the marine particles (namely phytoplankton and minerals) for different water conditions. Their analysis revealed that the use of the polarization of scattered energy in ocean color algorithms might significantly improve the retrieval of hydrosol properties, especially in coastal waters. It is the purpose of this study to investigate the potential of using the polarized reflectance in remote sensing algo-

[1]Université Pierre et Marie Curie-Paris 6, Laboratoire Océanographie de Villefranche, CNRS, Villefranche sur Mer, France.

0148-0227/07/2006JC003843$09.00

rithms to address the inverse problem of ocean color, thus extending the previous work of *Chami et al.* [2001]. First, the parameters used in the radiative transfer simulations are described. Then, the sensitivity of the water leaving radiation to the polarization effects induced by the marine particles is discussed for open ocean and coastal waters applications. Finally, remote sensing algorithms based on the polarized reflectance are proposed to retrieve the particulate concentration in the water mass.

2. Theoretical Background

[4] In order to describe the full polarization state of light propagating in a given direction, the Stokes vector convention is adopted. For a detailed explanation of the Stokes parameters, the reader is referred to *Van de Hulst* [1981]. The flux and polarization of a beam of light can be represented by a column vector $I_v = (I,Q,U,V)$ or Stokes vector. The four Stokes parameters I, Q, U, V characterize the energy transported by the electromagnetic wave, its degree of polarization, the direction of polarization and the ellipticity. The parameter I can be any energetic quantity, as a radiance, an irradiance, etc., and is generally named intensity. The parameters Q, U, V are defined, as is I, from the two components of the electric vector on two arbitrary perpendicular axis (x, y) in the wave plane. Q, U, V are quantities with the same energetic dimension as I. Generally, a reference plane is chosen through the direction of propagation; the x-axis is parallel to the reference plane and the y-axis perpendicular. The reference plane is taken as the vertical plane containing the direction of propagation.

[5] The polarized intensity I_p and the degree of polarization P are defined respectively as (equations (1) and (2)):

$$I_p = \sqrt{Q^2 + U^2 + V^2} \tag{1}$$

$$P = I_p / I \tag{2}$$

where $0 \leq P \leq 1$. The limit $P = 0$ corresponds to a completely unpolarized radiation field while $P = 1$ corresponds to a completely polarized radiation field. Radiation fields with intermediate values of P are partially polarized. Any field with a degree of polarization P can be represented as a linear combination of an unpolarized radiance $(1 - P)$ I and a completely polarized field of radiance PI, i.e. (equation (3)):

$$\begin{pmatrix} I \\ Q \\ U \\ V \end{pmatrix} = \begin{pmatrix} (1-P)I \\ 0 \\ 0 \\ 0 \end{pmatrix} + \begin{pmatrix} PI \\ Q \\ U \\ V \end{pmatrix} \tag{3}$$

[6] For natural light, $Q = U = V = 0$. Fields for which $V = 0$ are considered linearly polarized. In this latter case, $Q = I_p\cos(2\chi)$, $U = I_p\sin(2\chi)$, where χ is the angle between the direction of vibration and the x-axis. In atmospheric and oceanic problems, V generally remains very small ($V \sim 10^{-3}$ I) [*Kattawar et al.*, 1976; *Plass et al.*, 1976]. Therefore, V is often neglected and the circular polarization effects are thus ignored.

[7] If light is scattered by an ensemble of randomly oriented particles, the Stokes vector of the incident beam and the scattered beam are, for each scattering angle θ, related by a 4×4 scattering matrix. Thus, the action of the atmosphere-ocean system on I_v is to produce a new Stokes vector I' given by (equation (4)):

$$I' = M(\theta) I_v \tag{4}$$

where M is the scattering matrix (also called Mueller matrix). The scattering matrix M describes the action of the environment on I_v. The elements of the matrix contains information about the size parameter, refractive index and structure of the scatterers. Because the Stokes vector is defined in the meridian plane, the state of the photon is rotated from the initial meridian plane into the scattering plane, which is defined by the direction of incidence and the direction of scattering, before operation by the Mueller matrix occurs. Then, the final Stokes vector is rotated into the new meridian plane. The complete scattering operation is therefore a product of three matrices. The scattered Stokes vector I_s is expressed in terms of the operations and original Stokes vector as follows (equation (5)):

$$I_s = R(\psi_1) M(\theta) R(\psi_2) I_v \tag{5}$$

where R is the rotation matrix, ψ_1 and ψ_2 are the two rotation angles and θ is the scattering angle.

3. Radiative Transfer Simulations

[8] The influence of the hydrosols on the polarized signal exiting the water mass is studied based on radiative transfer modelling. The simulations were carried out using the OSOA model [*Chami et al.*, 2001], which solves the vector radiative transfer equation for the atmosphere-ocean system using the successive orders of scattering method and the Stokes formalism above described. This section reports the inputs parameters used in the computations. For a detailed description of the OSOA model, the reader is referred to *Chami et al.* [2001].

[9] The atmosphere corresponds to a mixture of molecules and aerosols. Standard atmosphere with maritime aerosols M70 having an optical depth τ_a of 0.2 at 570 nm (i.e., horizontal visibility of 23 km) is used to simulate the incoming solar light. The oceanic layer is described using a four component seawater model. The four components are pure seawater, phytoplankton pigments, inorganic suspended material (hereafter referred to as sediment) and colored dissolved organic matter *CDOM*. The inherent optical properties of marine constituents are modeled as follows. Pure seawater absorption spectral coefficients are taken from *Pope and Fry* [1997]. The absorption coefficient of *CDOM* a_{CDOM} is estimated using the exponential model provided by *Bricaud et al.* [1981] (equation (6)):

$$a_{CDOM}(\lambda) = a_{CDOM}(440) \exp[-0.014(\lambda - 440)] \tag{6}$$

where λ stands for the wavelength.

Table 1. Scattering (b_{ph}) and Backscattering (b_{bph}) Coefficients of Phytoplankton at 570 nm

Chl, mg m^{-3}	0.03	0.1	0.3	1	3	10	30
b_{ph}, m^{-1}	0.027	0.069	0.160	0.401	0.931	2.341	5.433
b_{bph}, m^{-1}	1.4 10^{-4}	3.5 10^{-4}	8.0 10^{-4}	2.0 10^{-3}	4.7 10^{-3}	1.17 10^{-2}	2.7 10^{-2}

[10] The absorption coefficient of phytoplankton and their covarying particles a_{ph} is calculated by use of the bio-optical model of *Bricaud et al.* [1998] (equation (7)):

$$a_{ph}(\lambda) = A_{ph}(\lambda)[Chl]^{Ep(\lambda)} \tag{7}$$

where *Chl* is the chlorophyll concentration (in mg m^{-3}), $A_{ph}(\lambda)$ and $E_p(\lambda)$ are tabulated coefficients. The phytoplankton scattering coefficient is modeled as suggested by *Loisel and Morel* [1998] (equation (8))

$$b_{ph}(\lambda) = 0.416[Chl]^{0.766}\left(\frac{550}{\lambda}\right) \tag{8}$$

[11] The refractive index of phytoplankton relative to water is 1.05. The size distribution of phytoplankton cells is assumed to follow the Junge hyperbolic function, which often is used for natural waters [*Bader*, 1970; *Carder et al.*, 1971; *Boss and Pegau*, 2001], with a Junge exponent value of −4. The minimum and maximum radii of the size distribution are 0.2 μm and 50 μm respectively. The optical properties of sediments are modeled using a complex refractive index of 1.16−0.001 *j* and a size distribution similar as phytoplankton. The Mueller matrix and thus, the total and polarized phase function of the particles, is computed by means of Mie theory.

[12] The OSOA model outputs the angular distribution of the radiance field and its degree of polarization at any desired level. In this paper, the bi-directional reflectance ρ (equation (9)) is calculated for three observations points: just beneath the sea surface (0^-), just above the sea surface (0^+) and at the top of the atmosphere (*TOA*).

$$\rho(\lambda) = \pi L_u(\theta_s, \theta_v)/E_d \tag{9}$$

[13] In equation (9), L_u is the upwelling radiance, E_d is the downwelling irradiance, θ_s and θ_v are the solar zenith angle and the viewing angle respectively. The unit of $\rho(\lambda)$ is sr^{-1}. The solar zenith angle is set up to 30°. All results are specified in the principal plane. The simulations are carried out at six wavelengths, namely 443 nm, 490 nm, 570 nm, 620 nm, 670 nm and 870 nm, which are commonly dedicated to ocean color analysis. The concentrations of phytoplankton and sediments used in the calculations are 0.03, 0.1, 0.3, 1, 3, 10, 30 mg m^{-3} and 1, 5, 10, 20, 30 mg l^{-1} respectively. The corresponding values of the scattering properties at 570 nm are reported in Tables 1 and 2. The values of $a_{CDOM}(440)$ are selected accordingly to the water type that is studied. $a_{CDOM}(440)$ is set up to 0.03 m^{-1} and 0.1 m^{-1} when dealing with open ocean waters and coastal areas respectively. A greater value is used for coastal waters applications owing to the river runoffs which induce an increase of the concentration of *CDOM*. Note that the $a_{CDOM}(440)$ values taken here are consistent with field observations previously reported by *Babin et al.* [2003].

4. Results and Discussion

[14] The sensitivity of the remotely sensed signal to the polarization effects of the marine particles is examined by analysing the variations in the polarized bi-directional reflectance ρ_{pol} with the turbidity of the water mass. To evaluate these variations, the absolute difference *AD* between the bi-directional reflectance calculated for a given concentration of suspended matter and the reflectance calculated for a concentration taken as a reference is calculated according to equation (10):

$$AD(SPM, x) = \Delta\rho_{pol}(SPM, x) = \left(\rho_{pol}(SPM_x) - \rho_{pol}(SPM_{ref})\right) \tag{10}$$

[15] In the notation used in equation (10), *SPM* stands for the water component (either *Chl* for phytoplankton or *sed* for sediment), *x* stands for the value of the particulate concentration and *ref* stands for the value of the particulate concentration taken as the reference. Here, the reference value of the concentration is 0.03 mg m^{-3} when *SPM* refers to *Chl,* and 1 mg l^{-1} when *SPM* refers to *sed*.

4.1. Sensitivity of the Polarized Reflectance to Phytoplankton in the Open Ocean

[16] The first case considered is the variation in ρ_{pol} with phytoplankton concentrations in open ocean waters. For this case, the sediment concentration is assumed to be negligible and thus, is set up to zero. In Figure 1, the subsurface polarized reflectance and the absolute difference *AD*(*Chl*, *x*) are plotted at 443 nm as a function of the viewing angle θ_v for various *Chl* concentrations. Note that in Figure 1 and other forthcoming similar figures, the range of angles where $\theta_v > 0$ corresponds to the specular plane (plane that does not contain the sun) and $\theta_v < 0$ corresponds the solar plane (where the sun is). It is observed that $\rho_{pol}(443)$ decreases as *Chl* increases. The absolute difference *AD*(*Chl*, *x* = 0.1 → 30 mg m^{-3}) (Figure 1b) can reach -7.10^{-3} sr^{-1} in the specular plane. Note that *AD* does not vary linearly with *Chl*; when *Chl* increases by one order of magnitude, *AD* vary within a factor of 3 (see for example the variations of *AD*(*Chl*, *x* = 0.3), *AD*(*Chl*, *x* = 3.0) and *AD*(*Chl*, *x* = 30) in Figure 1b). On the basis of equation (2), the variations in ρ_{pol} are directly related to variations in both the total

Table 2. Scattering (b_{sed}) and Backscattering (b_{bsed}) Coefficients of Sediments at 570 nm

Sed, mg l^{-1}	1	5	10	20	30
b_{sed}, m^{-1}	0.355	1.78	3.56	7.11	10.67
b_{bsed}, m^{-1}	1.0 10^{-2}	5.3 10^{-2}	1.1 10^{-1}	2.1 10^{-1}	3.2 10^{-1}

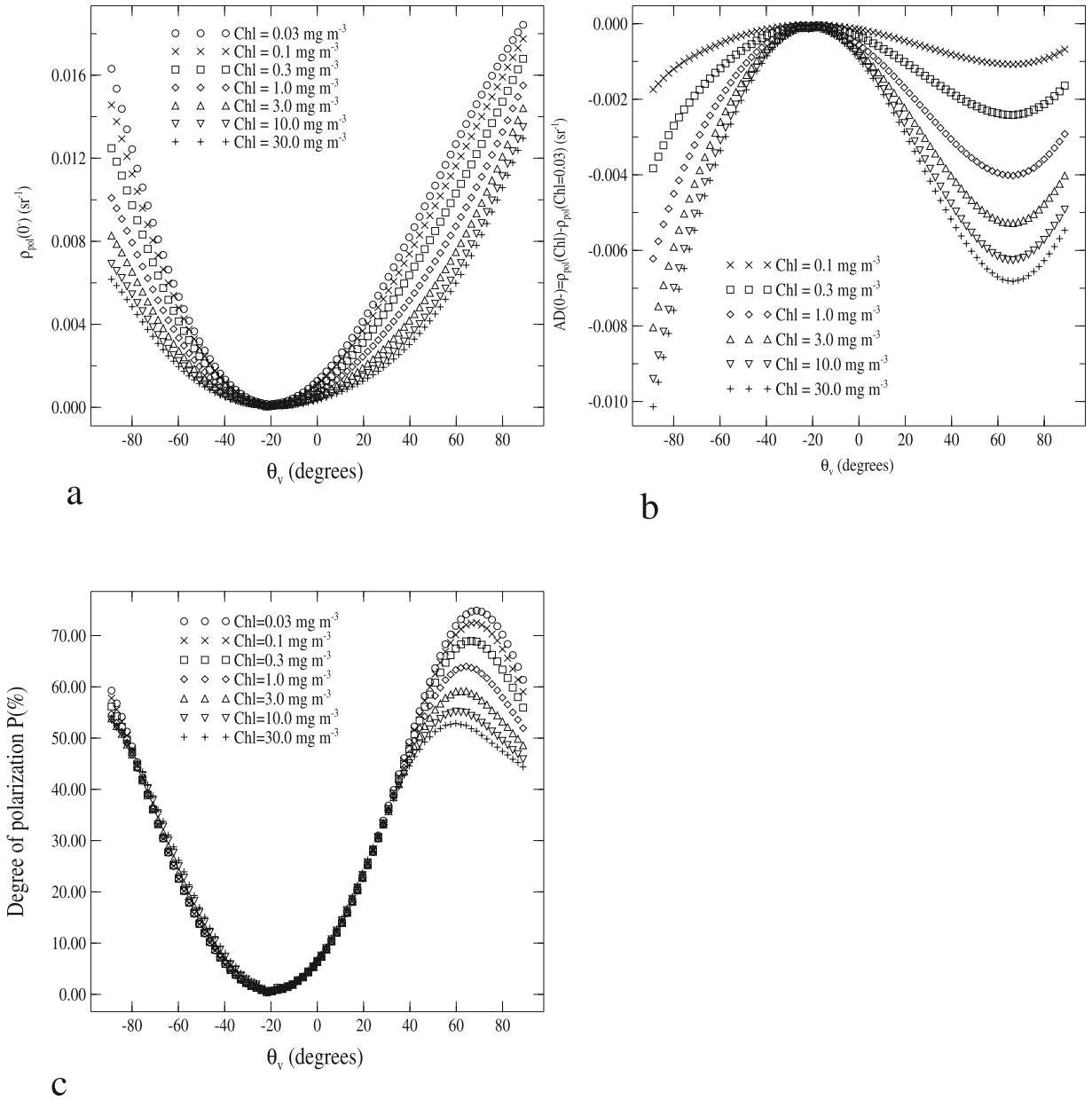

Figure 1. (a) Angular distribution of the polarized reflectance $\rho_{pol}(0^-)$ for different values of *Chl* concentrations, (b) absolute difference *AD* between $\rho_{pol}(0^-)$ at a given value of *Chl* and $\rho_{pol}(0^-)$ at the reference value of *Chl* = 0.03 mg m^{-3} (see equation (10)) and (c) angular variation of the degree of polarization *P* at 0^- for different values of *Chl* concentrations. The conditions of simulation are as follows: $\lambda = 443$ nm, $\theta_s = 30°$, $a_{CDOM}(440\text{ nm}) = 0.03\ m^{-1}$, $sed = 0$ mg l^{-1}, the aerosol model is M70 and the aerosol optical depth τ_a at 570 nm is 0.2. Note that the half plane $\theta_v > 0$ is the specular plane and the half plane $\theta_v < 0$ is the solar plane.

reflectance and the degree of polarization. The magnitude of the total reflectance decreases at 443 nm due to phytoplankton absorption, thus inducing negative values of $AD(Chl, x)$. The degree of polarization is typically characterized by a "bell-shape" (Figure 1c) with neutral points (i.e., points where the degree of polarization is zero) at a scattering angle of 180° ($\theta_v \sim -20°$) and a maximum value (noted $P_{\max}$) at a scattering angle around 90°–100° ($\theta_v \sim +70°$). The angular shape of ρ_{pol} and $AD(Chl, x)$ closely follows that of the degree of polarization inasmuch as the lowest values are observed in the backscattering region while the highest values occur at right-angle scattering. As shown in Figure 1c, the degree of polarization *P* is sensitive to the turbidity of the water mass; *P* non linearly decreases ($P_{\max}$ varies from 75% to 52%) as *Chl* increases. The polarization of the radiation is an intrinsically single scattering phenomenon which is primarily due to the molecular scattering. However, the polarization is significantly attenuated by multiple scattering processes. The turbid waters, which are characterized by a prevailing multiple-scattering regime,

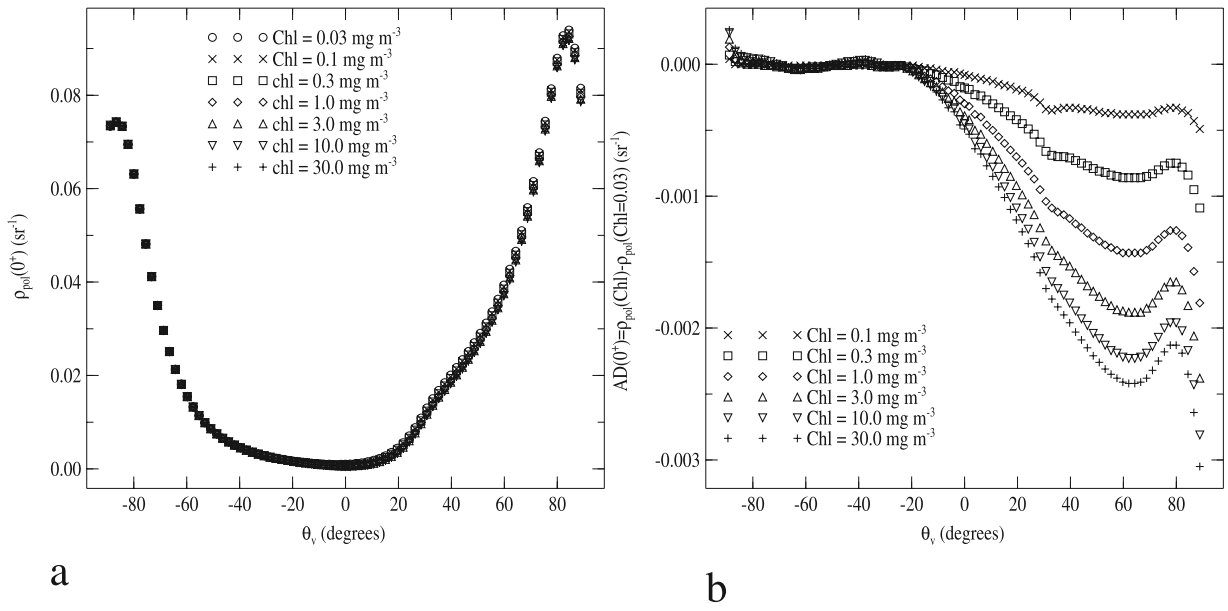

Figure 2. (a) Same as Figure 1a except the observation is made at 0^+. (b) Same as Figure 1b except the observation is made at 0^+.

thus contribute to strongly depolarize the radiation, as observed in Figure 1c for high *Chl* values. At 443 nm, the multiple scattering adding further to the absorption effects thus explain the significant decrease of ρ_{pol} with *Chl*. At 570 nm, because the absorption by phytoplankton is weak, the variations in the polarized reflectance are mostly due to scattering processes. Despite a stronger depolarisation of the signal ($P_{\max}$ varies from 82% to 48%) than that at 443 nm, ρ_{pol} significantly increases with *Chl* (up to a factor of 2, not shown). The depolarisation effects are compensated by the increase of the magnitude of the total reflectance, which is thus the major contributor to the variations in $\rho_{pol}(570)$. At longer wavelengths, despite its lower magnitude, the polarized signal is still significantly influenced by phytoplankton.

[17] The variations in ρ_{pol} with *Chl* just above the ocean surface (i.e., 0^+) are next considered in Figure 2. The polarized reflectance is slightly sensitive to *Chl* (Figure 2a). The absolute difference $AD(Chl, x = 0.1 \rightarrow 30)$ at 443 nm shows maximum values in the specular plane (Figure 2b). The effect of the ocean properties on the polarized reflectance is drastically reduced (typically by a factor of 6) when comparing with the observations at 0^-. Note that in the solar plane ($\theta_v < 0$), the polarized reflectance is fairly insensitive to *Chl*. The polarization pattern in the upwelling light above the surface is due to reflected skylight and light transmitted from beneath the surface of the ocean. The reflected skylight radiation is theoretically totally polarized at the Brewster angle ($\theta_v = +54°$). However, because of the contribution to the light field from light scattered beneath the surface and transmitted through the boundary, the maximum degree of polarization at 0^+ is less than 100%. The amount of hydrosols in the water must be appreciable before a change in the polarized reflectance above the surface can be observed. The calculation of the relative difference $RD(Chl, 0.1 \rightarrow 30 \text{ mg m}^{-3}) = AD/\rho_{pol}$, at the Brewster viewing angle (Figure 3) shows that the sensitivity of $\rho_{pol}(0^+)$ to *Chl* is smaller than 3% in waters out of bloom conditions (i.e., $Chl < 0.3 \text{ mg m}^{-3}$). Since such waters represent roughly 80% of the entire open ocean waters [*Antoine et al.*, 1996], it appears that above water polarized measurements are not necessarily relevant to derive information on the biomass concentration at the global scale.

[18] At the top of atmosphere (Figure 4a), the absolute difference $AD(Chl, x = 0.1 \rightarrow 30 \text{ mg m}^{-3})$ significantly decreases compared to that of the previous cases. The relative difference *RD* at the right-angle scattering is smaller

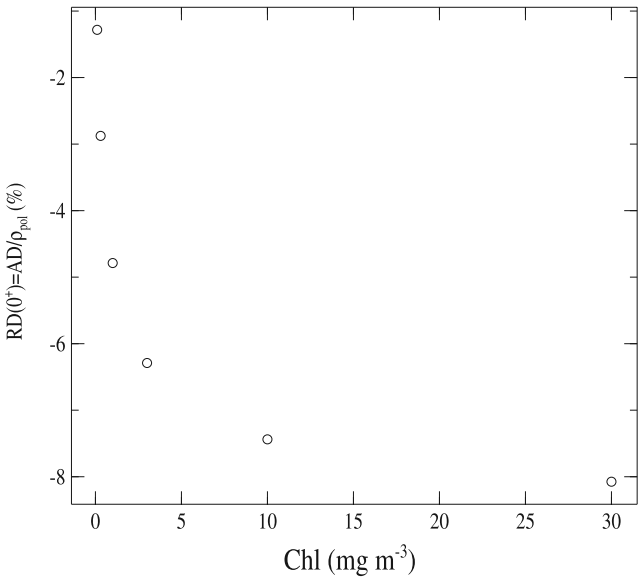

Figure 3. Relative difference $RD = AD/\rho_{pol}$ (in %) between the polarized reflectance at a given value of *Chl* (corresponding to the *x*-axis) and a reference value of *Chl* (i.e., $Chl_{ref} = 0.03 \text{ mg m}^{-3}$). The calculation is carried out at 443 nm, at the Brewster viewing angle (i.e., $\theta_v = +54°$) and at 0^+.

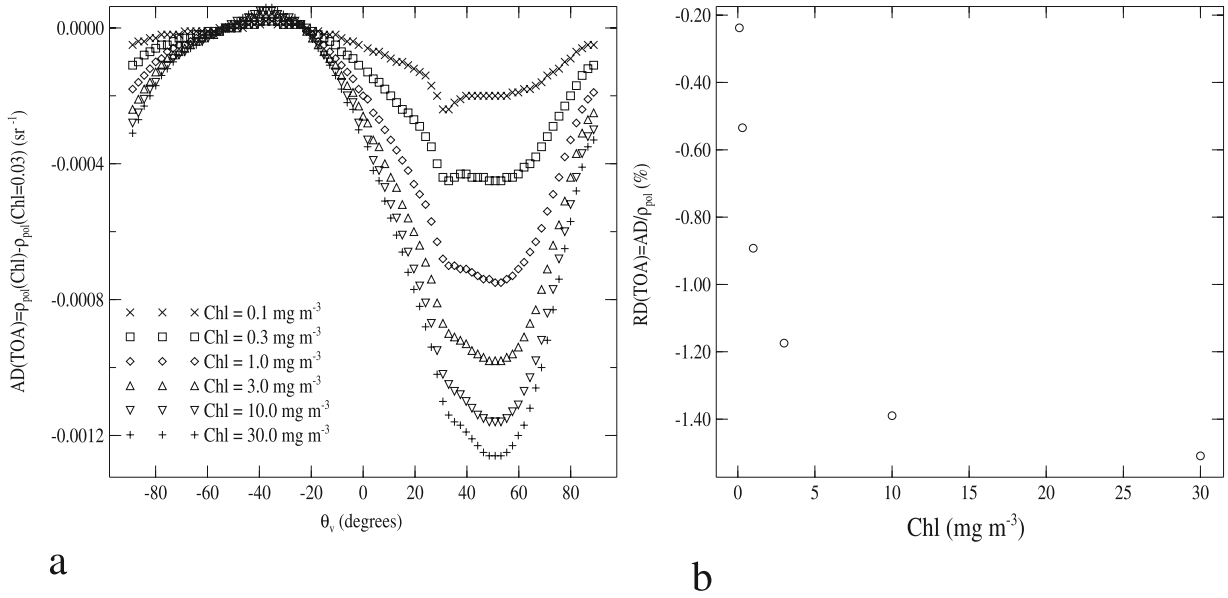

Figure 4. (a) Absolute difference *AD* between $\rho_{pol}(TOA)$ at a given value of *Chl* and $\rho_{pol}(TOA)$ at the reference value of *Chl* = 0.03 mg m^{-3} (see equation (10)) at 443 nm. The conditions of simulation are already mentioned in Figure 1. (b) Relative difference $RD = AD/\rho_{pol}$ (in %) between the polarized reflectance at a given value of *Chl* (corresponding to the *x*-axis) and a reference value of *Chl* (i.e., Chl_{ref} = 0.03 mg m^{-3}). The calculation is carried out at 443 nm, at the Brewster viewing angle (i.e., θ_v = +54°) and at *TOA*.

than 1.5% (Figure 4b), which is about 4 times less than at 0^+. Note that similar results were obtained at other wavelengths. The reason for this decrease of *RD* is the total contribution to the radiance and degree of polarization at the top of atmosphere is predominantly from the atmospheric layer. In particular, the molecular Rayleigh scattering plays a major role since it strongly polarizes the diffuse radiation. Therefore, the atmosphere tends to highly reduce the effects of both the air-water interface and the ocean parameters. Calculations carried out for different levels of atmospheric turbidity (Figure 5) confirm that ρ_{pol} is weakly sensitive to the variations in *Chl*, even for clear atmosphere ($RD(Chl, x = 30 \text{ mg m}^{-3}) < 1.8\%$). Other simulations showed that the solar zenith angle and azimuth has a little influence on these results. The implications for remote sensing of ocean color are important. Based on Figure 4a, when *Chl* is lower than 0.3 mg m^{-3}, $\Delta\rho_{pol}$ is smaller than 4.10^{-4} sr^{-1}, which is typically within the noise equivalent reflectance of usual ocean color satellite sensors [*IOCCG*, 1998; *Antoine and Morel*, 1999]. Thus, ρ_{pol} is virtually insensitive to *Chl* in waters out of bloom conditions. It is interesting to note that this holds true at other wavelengths. Therefore, the polarized signal at the top of atmosphere can be efficiently used in the visible bands to improve the characterization of the aerosols in the open ocean waters regardless of the oceanic turbidity, thus supporting the results recently obtained by *Chowdhary et al.* [2006]. More specifically, polarized channels in the visible bands could be of great interest in the atmospheric correction algorithms. Currently the aerosol model in any atmospheric correction algorithms is derived based on the total reflectance measured in the near infrared bands. The atmospheric signal at shorter wavelengths is obtained applying the spectral dependency of the retrieved aerosol model and extrapolating the aerosol reflectance from the near infrared to the visible bands. Such an extrapolation may lead to an overestimation of the atmospheric component and to the retrieval of negative values of the water leaving radiances.

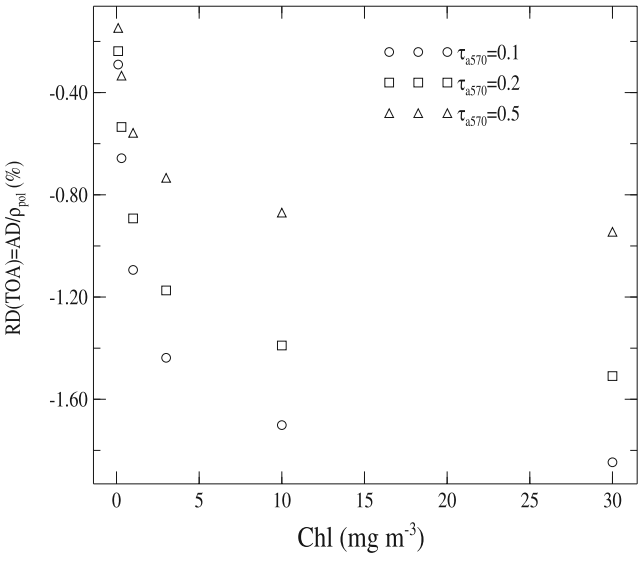

Figure 5. Relative difference $RD = AD/\rho_{pol}$ (in %) between the polarized reflectance at a given value of *Chl* (corresponding to the *x*-axis) and a reference value of *Chl* (i.e., Chl_{ref} = 0.03 mg m^{-3}) for different values of the aerosol optical depth τ_a at 570 nm. The calculation is carried out at 443 nm, at the Brewster viewing angle (i.e., θ_v = +54°) and at *TOA*.

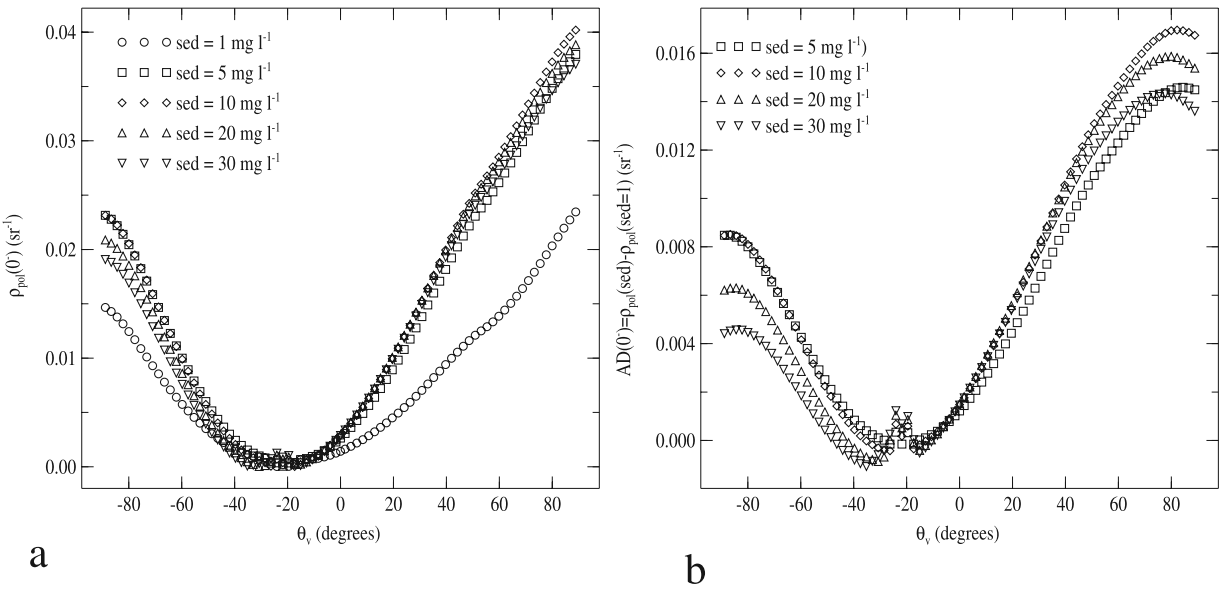

Figure 6. (a) Angular variations of the polarized reflectance ρ_{pol} at 0^- and $\lambda = 570$ nm for different *sed* concentrations. (b) Absolute difference *AD* between $\rho_{pol}(0^-)$ at $\lambda = 570$ nm at a given value of *sed* and $\rho_{pol}(0^-)$ at the reference value of *sed* = 1 mg l^{-1} (see equation (10)). The conditions of simulation are as follows: $\theta_s = 30°$, $\tau_a(570\text{ nm}) = 0.2$, $a_{CDOM}(440) = 0.1\ m^{-1}$, *Chl* = 1 mg m^{-3}.

This study shows that the polarized channel in the blue can be used together with red channels to better adjust the spectral dependency of the aerosol model, thus improving the quality of the atmospheric correction and the determination of the water leaving radiance. However, it should be highlighted that such an approach may be carefully applied when dealing with bloom conditions because of the greater sensitivity of ρ_{pol} to *Chl*. For these latter cases, the selection of appropriate viewing angles where the sensitivity vanishes (region where $\theta_v < 0$ in Figure 4a) is necessary to address the problem. These results are highly encouraging in the prospect of the exploitation of the polarized and multi-angular data collected by the satellite sensor PARASOL (CNES) that still remains to be achieved.

4.2. Sensitivity of the Polarized Reflectance to the Suspended Matter in Coastal Waters

[19] The variations in ρ_{pol} with the particulate suspended matter in coastal waters are now examined. Because of the influence of rivers runoffs in these areas, the contribution to the optical properties of the particles from highly refractive materials may be significant. Therefore, the influence of the sediments on the polarized signal is primarily investigated. The value of the *Chl* concentration is fixed to 1 mg m^{-3}.

[20] Figure 6 shows the variations in ρ_{pol} beneath the surface at 570 nm for various sediment concentrations. The magnitude of the polarized reflectance significantly increases with the concentration in the specular plane (Figure 6a). The absolute differences $AD(sed,\ x = 5 \rightarrow 30\text{ mg } l^{-1})$ are maximum around $\theta_v \sim +60°$ (Figure 6b), which is close to the right-angle scattering. This is consistent with the fact that the degree of polarization is the most sensitive to the turbidity of the water at the scattering angle where *P* is maximum, as previously shown in the case of phytoplankton (see Figure 1c). Therefore, the measurement of the polarized bi-directional reflectance near the right-angle scattering is interesting and appropriate to characterize the water mass in terms of particle concentrations. Figure 7 shows the relative difference $RD(sed,\ x = 5 \rightarrow 30\text{ mg } l^{-1})$ between $\rho_{pol}(sed)$ and $\rho_{pol}(sed = 1\text{ mg } l^{-1})$ at a scattering angle of 100° and for different wavelengths. The relative difference can vary

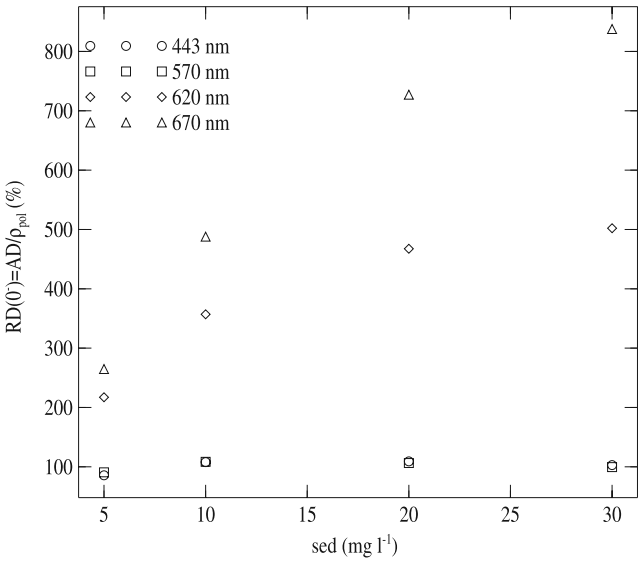

Figure 7. Relative difference $RD = AD/\rho_{pol}$ (in %) between the polarized reflectance at a given value of *sed* (corresponding to the *x*-axis) and a reference value of *sed* (i.e., sed_{ref} = 1 mg l^{-1}) for different wavelengths. The conditions of simulation are as follows: $\theta_s = 30°$, scattering angle $\theta = 100°$, $\tau_a(570\text{ nm}) = 0.2$, $a_{CDOM}(440) = 0.1\ m^{-1}$, *Chl* = 1 mg m^{-3}. The observation is made at 0^-.

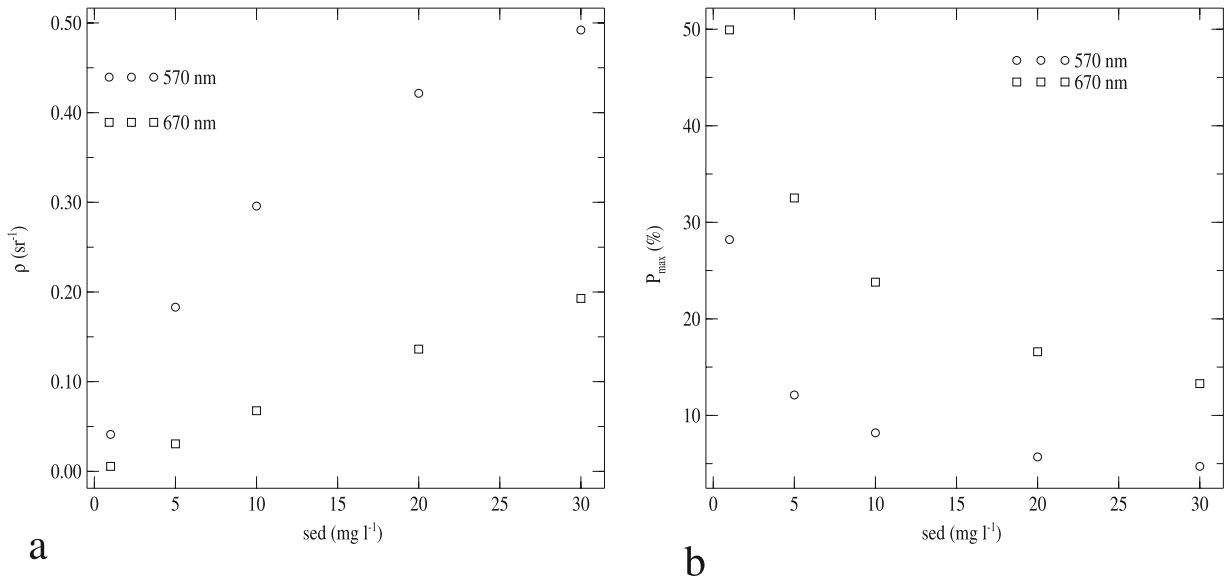

Figure 8. (a) Variations in the total bi-directional reflectance as a function of *sed* concentration. (b) Variations in the degree of polarization $P_{\max}$ as a function of *sed* concentrations. The condition of simulation are as follows: $\theta = 100°$, $\lambda = 570$ nm and 670 nm, the observation is made at 0^-, $\theta_s = 30°$, $\tau_a(570\text{ nm}) = 0.2$, $a_{CDOM}(440) = 0.1\ \text{m}^{-1}$, $Chl = 1\ \text{mg m}^{-3}$.

from 100% to 800% according to the wavelength. However, at 443 nm and 570 nm, the sensitivity of ρ_{pol} to the sediment concentration is very weak (i.e., the variations of *RD* with *sed* are relatively flat) compared with the other channels. At these short wavelengths, it is difficult to discriminate the sediment concentration from ρ_{pol}, as also observed in Figure 6a. The magnitude of the total reflectance ($\sim$0.50 sr^{-1} when *sed* = 30 mg l^{-1} at 570 nm) is so high (Figure 8a) that it leads to the saturation of the polarized reflectance, despite the significant depolarisation of the signal resulting from the increase of the multiple scattering events (Figure 8b). At longer wavelengths (for example at 670 nm), the magnitude of the total reflectance is significantly lower than that at 570 nm (Figure 8a) as expected from the increased absorption by pure seawater. The polarized reflectance is thus more sensitive to sediment loading. The polarized reflectance at long wavelengths could then be informative on the water content in suspended matter. This aspect will be discussed later.

[21] The above water polarized reflectance is highly variable with the sediment concentrations (Figure 9). As depicted in Figure 9, the relative difference *RD*(*sed*, 1 $\rightarrow$ 30 mg l^{-1}) at a scattering angle of 100° reaches 40% in the most turbid case, which is five times greater than what was observed in the case of phytoplankton dominated waters (Figure 3). ρ_{pol} is more sensitive to the particulate content of the water mass when the latter is dominated by sediment rather than phytoplankton. Such a result is expected for two reasons. The first is that the probability of backscattering by sediments is much higher, as shown in Figure 10. Therefore, the photons scattered by inorganic matter will affect more significantly the upwelling light field and thus, the polarized reflectance. The second reason is that the amount of sediments in the water is sufficiently appreciable ($\rho_{pol}(0^-)$ at 670 nm is about 0.04 sr^{-1} at the right-angle scattering when *sed* = 30 mg l^{-1}) to induce changes in the polarization pattern above the surface despite the significant scattering by the overlying atmosphere. The implications for the correction of the total reflectance measured just above the sea surface for the skylight reflection effects using the polarized signal are important. Based on the theoretical finding that the spec-

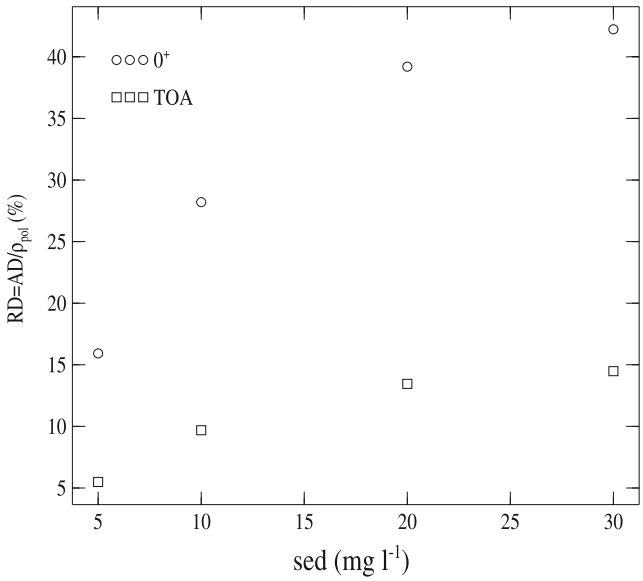

Figure 9. Relative difference $RD = AD/\rho_{pol}$ (in %) between the polarized reflectance at a given value of *sed* (corresponding to the *x*-axis) and a reference value of *sed* (i.e., $sed_{ref} = 1$ mg l^{-1}) when the observation is made at 0^+ and *TOA*. The condition of simulation are as follows: $\theta = 100°$, $\lambda = 670$ nm, $\theta_s = 30°$, $\tau_a(570\text{ nm}) = 0.2$, $a_{CDOM}(440) = 0.1\ \text{m}^{-1}$, $Chl = 1\ \text{mg m}^{-3}$.

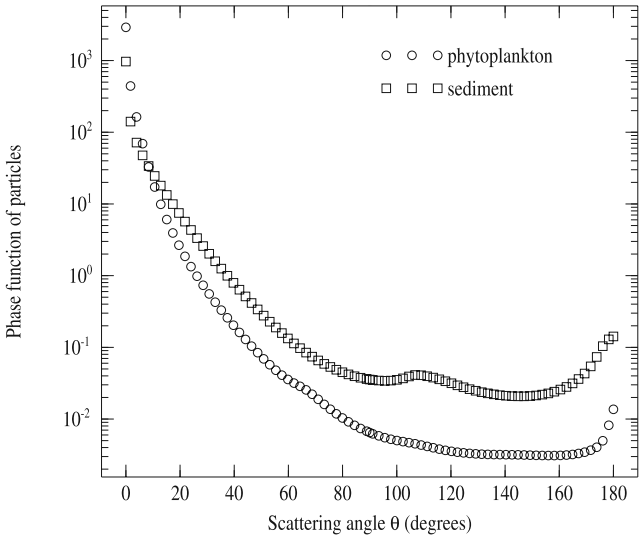

Figure 10. Phase functions of phytoplankton and sediment.

ular reflection of the sky radiance at the air-sea interface is totally perpendicular polarized at the Brewster viewing angle (i.e., $P_{max} = 1$), *Fougnie et al.* [1999] proposed to significantly reduce the contribution to the reflectance from the skylight reflection measuring the parallel component of the upwelling signal. The underlying assumption is that the radiance scattered by the ocean does not significantly alter the polarization state of light at 0^+. *Fougnie et al.* [1999] verified this latter assumption in the case of open ocean waters only. Note that the weak sensitivity of $\rho_{pol}(0^+)$ with *Chl* previously observed in this study (see Figure 3) also corroborates the fact that the method proposed by *Fougnie et al.* [1999] is relevant and applicable for the majority of the open ocean waters (i.e., out of bloom conditions). To highlight the influence of the sediment on the polarization state of light, the variations in P_{max} above the sea surface are plotted as a function of the sediment concentration (Figure 11). P_{max} varies from 94% to 20% as the concentration increases. A high value of $P_{max}(0^+)$ is expectedly observed in clear waters (i.e., *sed* = 1 mg l^{-1}) because of the prevailing contribution to the reflectance from the skylight reflection at the interface compared to the contribution from the signal exiting the ocean. However, Figure 11 shows that a significant amount of highly refractive particles in the water mass induce a strong depolarisation of the signal (up to 74%), thus meaning that the reflectance measured by a radiometer viewing the ocean just above the sea surface is not totally perpendicular polarized in these conditions. The interaction of the light transmitted from beneath the surface with the reflected skylight radiation strongly modifies the polarization signature of the upwelling signal reaching the sensor such that the skylight reflection component could not be easily separated from the water component. Therefore, the approach that consists of using the parallel-polarized signal to minimize the skylight reflection effects such as that proposed by *Fougnie et al.* [1999] should be carefully applied in turbid waters. Based on Figure 11 such an approach can be as far as 74% inaccurate at 670 nm and even more important at shorter wavelengths due to the higher depolarisation process caused by the increased level of water leaving radiance.

[22] At the top of atmosphere, the relative difference $RD(sed, 1 \rightarrow 30 \text{ mg } l^{-1})$ between $\rho_{pol}(sed)$ and $\rho_{pol}(sed = 1 \text{ mg } l^{-1})$ at the scattering angle of 100° (Figure 9) varies from 5% to 15%. Similar range of variations are observed at other wavelengths. As expected, the atmosphere tends to reduce the effects of both the interface and the water mass. However, the sensitivity of $\rho_{pol}(TOA)$ to suspended matter is still significant with regard to remote sensing applications. Contrary to the case of phytoplankton dominated waters where the sensitivity was smaller than 3% (see section 4.1), it is clearly not relevant here to exploit the polarized channels in the visible and spectral bands to improve atmospheric correction algorithms or aerosol retrieval in coastal zones.

4.3. Ocean Color Algorithms Based on the Polarized Reflectance

[23] Different approaches are currently applied to address the inversion problem of ocean color. The empirical approach, which consists in establishing statistical relationships between the total (i.e., unpolarized) reflectance and the biogeochemical parameters, has been shown to be efficient in open ocean waters [*O'Reilly et al.*, 1998] and inappropriate in coastal waters due to overlapping optical signatures of phytoplankton and inorganic matter. In this latter case, semi-analytical algorithms appeared to be more robust [*Tassan*, 1994; *Moore et al.*, 1999; *Chami and Robilliard*, 2002]. As discussed above, the polarization can provide relevant physical information on the optical properties of the suspended matter in coastal zones. Therefore, the polarized reflectance might be used as an alternative approach to derive biogeochemical parameters in optically complex waters. Here, it is investigated whether a simple empirical algorithm based on the polarized reflec-

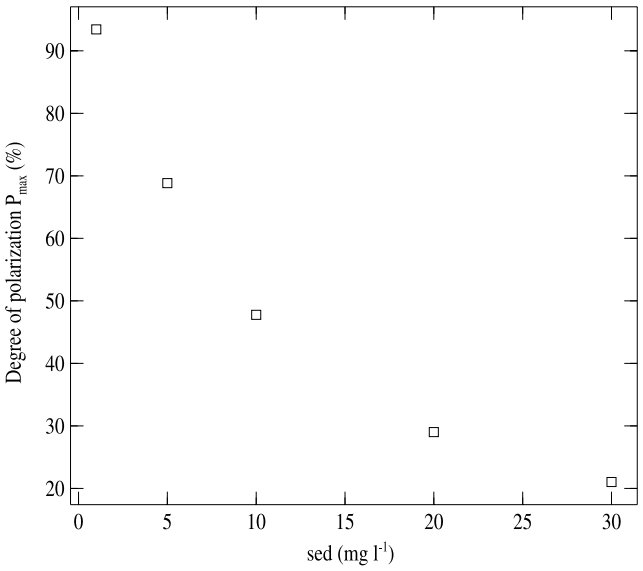

Figure 11. Degree of polarization P_{max} as a function of *sed*. The observation is made at 0^+ and at $\lambda = 670$ nm. The other conditions of simulation are already mentioned in Figure 9.

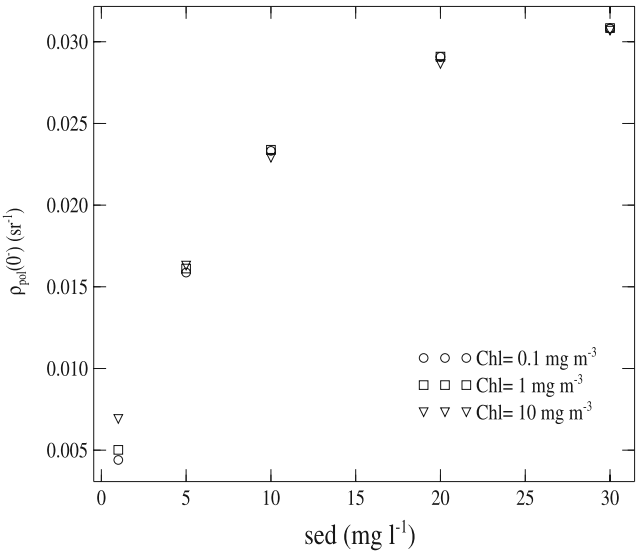

Figure 12. Polarized reflectance $\rho_{pol}(0^-, \theta = 100°)$ at λ = 620 nm as a function of *sed*. The variations with *Chl* are also reported.

tance might be successful to estimate the particulate concentration in coastal areas. Since the polarized reflectance beneath the surface at long wavelengths was previously observed not to be saturated when the amount of sediment is high, the relationship between $\rho_{pol}(0^-)$ at the right-angle scattering at 620 nm and the sediment concentration is studied first (Figure 12). ρ_{pol} is not only highly sensitive to the turbidity but also shows a significant magnitude. Typically, $\rho_{pol}(0^-)$ varies from 0.005 sr^{-1} to 0.03 sr^{-1} within the range of variation of the sediment concentration. Similar observations were made at 670 nm. Therefore, the polarized reflectance at long wavelengths can be potentially used in ocean color algorithms to retrieve the suspended matter concentration in turbid waters. Note, however, that an appropriate viewing geometry should be adopted (i.e., at the angle where the polarization is maximum). This means that multi-angular measurements of the polarized reflectance are necessary. Because of the significant variability of the *Chl* concentration that occurs in coastal waters, especially during bloom events, the influence of *Chl* on the algorithm is examined (Figure 12). The polarized reflectance remains virtually insensitive to *Chl*, despite a variation of *Chl* within 2 orders of magnitude. Because the backscattering efficiency of sediments is much greater than that of phytoplankton (see Figure 10), the photons scattered by inorganic particles predominantly contributes to the upwelling signal. On the other hand, since the scattering phase function of biogenic particles is more highly forward peaked than that of sediments, the photons scattered by phytoplankton continue travelling deeper into the ocean thus slightly affecting the upwelling light field. Therefore, the influence of phytoplankton on the polarized reflectance when the sediments are present in the water mass is very weak. This means that the polarized reflectance at long wavelengths might allow the separation of the optical signature of inorganic particles from that of biogenic particles, as previously inferred by *Volten et al.* [1998]. It is currently well established that the unpolarized reflectance measured in the red and near infrared bands can be used in coastal zones to estimate the total amount of suspended matter (phytoplankton and sediments) [*Doxaran et al.*, 2002; *Ruddick et al.*, 2006]. This is because the unpolarized reflectance is sensitive to variations of both phytoplankton or sediment. Here, it is shown that additional polarization measurements can be highly informative on the composition of the particles (i.e., refractive index) present in the water mass. The total and polarized reflectance are thus both complementary physical properties. Their simultaneous use should significantly improve the performance of inversion algorithms in optically complex waters.

[24] The current empirical ocean color algorithms are often based on a spectral ratio of reflectance to reduce the effects of the uncertainty in the measurements but also to enhance the sensitivity of the algorithm to suspended matter. Such a method is exclusively applied for open ocean waters. Here, a band ratio approach using polarization is investigated for applications in coastal zones. The development of a band ratio algorithm necessitates finding a hinge point in the reflectance spectrum. It was previously shown (section 4.2) that the polarized signal is nearly saturated at short wavelengths (443 nm and 570 nm) in turbid waters; i.e. ρ_{pol} was fairly insensitive to the sediment concentration when *sed* > 1 mg l^{-1}. An attempt is then made to use the polarized reflectance at one of these wavelengths as a hinge point. Note, however, that the selection of the hinge point also requires that ρ_{pol} should not be sensitive to variations in *Chl* concentration too. This latter condition was correctly verified at 570 nm. At 443 nm, the sensitivity of ρ_{pol} to *Chl* was too high (~30%) to meet the requirement. Therefore, the polarized reflectance at 570 nm is used together with the polarized reflectance at 620 nm as a spectral band ratio algorithm. Results show (Figure 13a) that the ratio ρ_{pol}(620 nm)/ρ_{pol}(570 nm) is highly sensitive to the sediment concentration while virtually neutral with regard to *Chl* in turbid water mass (*sed* > 1 mg l^{-1}). Similar features were observed regarding the ratio ρ_{pol}(670 nm)/ρ_{pol}(570 nm). To evaluate the influence of the polarization on the algorithm, the spectral ratio of the unpolarized reflectance at 620 nm and 570 nm is related to the sediment concentration (Figure 13b) and compared to the polarized algorithm. The influence of *Chl* on the retrieval of *sed* in the case of the unpolarized-based approach is much greater than that observed for the polarized algorithm. As an example, when the ratio of total reflectance is equal to 0.4 (see Figure 13b), the estimates of *sed* varies within a factor of 2, from 5 to 10 mg l^{-1}, depending on the *Chl* concentration. Such a significant uncertainty does not appear in the case of the polarization-based algorithm. The band ratio polarized algorithm proposed here, despite its straightforwardness, can be efficient to estimate the amount of suspended inorganic material in coastal waters. Given the uncertainty in the reflectance measurements, the sensitivity of the band ratio polarized algorithm to noise is studied. The simulated reflectance is disturbed by adding 5% noise at 570 nm, which typically corresponds to the radiometric performance of the available instruments. The uncertainty in the spectral shape of the reflectance is also taken into account assuming a greater noise in the reflectance at 620 nm than that at 570 nm. A greater noise can be expected in the red band because of the lower magnitude of the signal exiting the

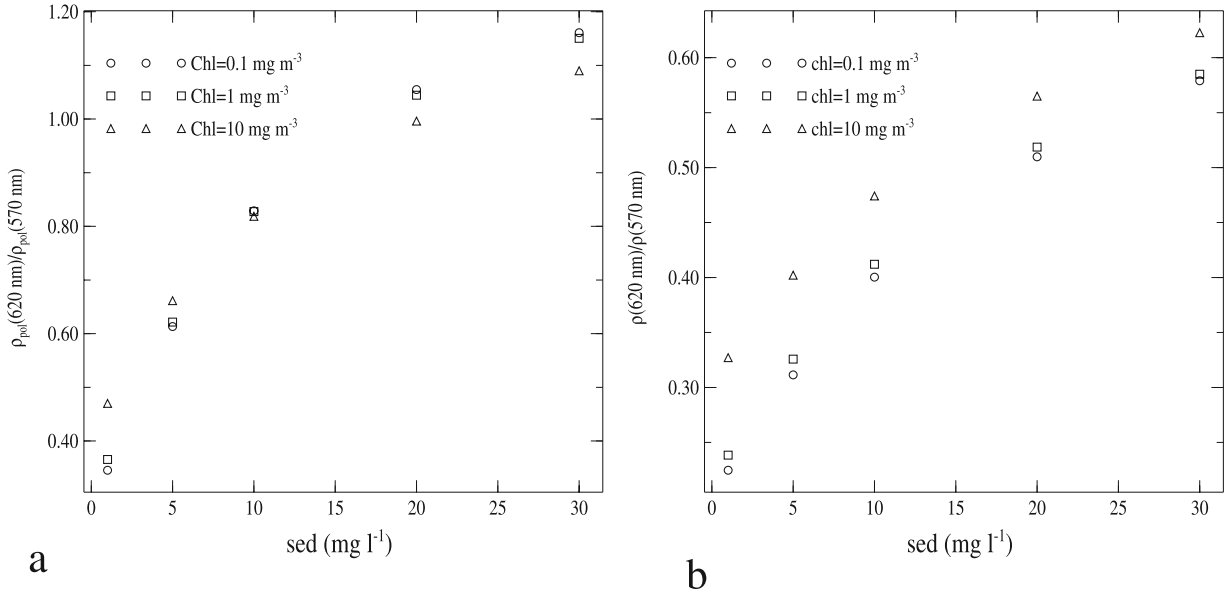

Figure 13. (a) Spectral ratio $\rho_{pol}(620\text{ nm})/\rho_{pol}(570\text{ nm})$ as a function of *sed*. The calculation is made at 0^-, $\theta = 100°$ and for different values of *Chl* (i.e., *Chl* = 0.1, 1 and 10 mg m^{-3}). (b) Similar as Figure 13a except the spectral ratio of the total reflectance $\rho(620\text{ nm})/\rho(570\text{ nm})$ is plotted.

ocean. The noise in the reflectance at 620 nm is thus increased by 10%, 30% and 50% relatively to the noise in the reflectance at 570 nm. The performance of the algorithm to retrieve the *sed* concentration is evaluated using the relative root mean square error (*RRMS*) (which is defined in the Notation section). The results show that the impact of noise on the retrieval of *sed* is lower than 10% (Table 3). Thus, the algorithm is fairly robust to uncertainties in the measurements. However, it should be highlighted that a degradation of the performance of the algorithm is expected when dealing with field data.

[25] The polarization-based empirical approach is also studied in the case of open ocean waters. The blue-green polarized reflectance ratio is related to *Chl* (Figure 14). As expected from Figure 1, the algorithm is highly sensitive to the variations in phytoplankton biomass. However, the comparison with the algorithm using the total reflectance, which is commonly used in the literature, shows virtually no differences between both methods. Other types of algorithms were tested (such as those based on the blue-red ratio or the blue-green difference) and led to similar results. Therefore, the polarization does not provide any additional relevant information to improve the retrieval of *Chl* in open ocean waters. Contrary to what was observed in coastal waters, the polarization is not a key issue to address the inversion problem in the global ocean. As suggested in section 4.1, the polarization might be a much more useful physical constraint for atmospheric correction algorithms in this type of water.

5. Conclusion

[26] In this paper, the importance of the polarization of the light field in the characterization of the oceanic constituents was analysed using radiative transfer calculations. Simulations were carried out for both open ocean and coastal waters conditions. First, the influence of phytoplankton and highly refractive material on the polarized reflectance was studied. Second, ocean color algorithms based on the polarization were investigated to retrieve the suspended matter concentration. There are several important results that I would like to emphasize. In open ocean waters, despite a great sensitivity to the chlorophyll concentration beneath the sea surface, the polarized reflectance at the top of atmosphere was observed to be fairly independent of the water content; the variations induced by *Chl* at this level were typically within the noise equivalent reflectance of satellite sensors. The reason is that the contributions to the polarization state of light from the air-water interface and the atmosphere are prevailing compared to that of phytoplankton cells. This result suggested that the polarized signal, including at short wavelengths, could be used for atmospheric correction purposes. In particular, polarization together with the total signal should allow a better determination of the spectral variation of the aerosol model. In coastal waters, the influence of the sediment on the degree of the polarization and on the magnitude of the reflectance was much greater than that of phytoplankton. Despite the smoothing effect induced by the interface and the atmospheric particles on the polarization state of light, the contribution to the polarized radiation from the oceanic particles was sufficiently significant to affect both the above water and top of atmosphere signals. Two conclusions can

Table 3. Sensitivity of the Retrieval of the Sediment Concentration to Noise-Contaminated Reflectance When the Band Ratio Polarized Algorithm $\rho_{pol}(620\text{ nm})/\rho_{pol}(570\text{ nm})$ Is Used[a]

Δ, %	10	30	50
RRMS, %	1.51	4.65	7.92

[a]The reflectance at 570 nm is disturbed by adding a 5% noise. The noise introduced in the reflectance at 620 nm is increased by a factor of Δ (in %) compared to the noise introduced in the reflectance at 570 nm. The performance of the retrieval of *sed* is evaluated using the *RRMS* (in %).

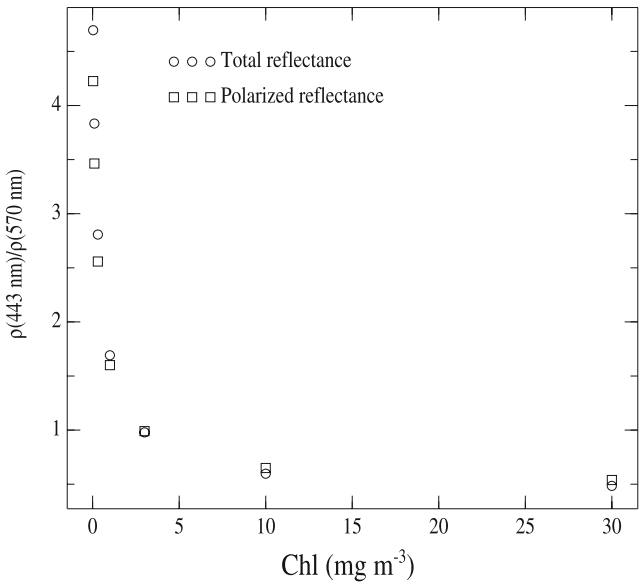

Figure 14. Spectral ratio $\rho_{pol}(443\text{ nm})/\rho_{pol}(570\text{ nm})$ and $\rho(443\text{ nm})/\rho(570\text{ nm})$ as a function of *Chl*. The calculation is made at 0^-, $\theta = 100°$, $sed = 0$ mg l^{-1}, $\theta_s = 30°$, $\tau_a(570\text{ nm}) = 0.2$, $a_{CDOM}(440) = 0.03$ m^{-1}.

be drawn from this latter result. The first is that the methodology that consists of using the polarized reflectance above the sea surface to reduce the skylight reflection effects should be carefully applied when dealing with turbid waters. The second is that the measurement of the polarization of scattered energy can be an alternative approach to the retrieval of hydrosol optical properties, which are currently based on intensity-only approach.

[27] Ocean color polarization-based algorithms were investigated. Only empirical approaches were tested as a feasibility study. In coastal areas, the analysis revealed that the polarized reflectance at wavelengths greater or equal to 570 nm is highly dependent on the sediment concentration, thus demonstrating that the polarization measurement can be potentially used to estimate the amount of inorganic material. The empirical algorithm was also virtually insensitive to the chlorophyll concentration. This suggested that polarization is a relevant physical constraint that can be used to separate the inorganic and biogenic component from the total suspended matter. Contrary to total intensity based algorithms, straightforward polarization-based algorithms might be successful in coastal zones. In open ocean waters, the results showed that an empirical polarized approach may also be relevant to retrieve *Chl* but no more improvement was observed compared to the total intensity approach.

[28] The potential of using the polarized signal to improve the retrieval of suspended matter concentration in optically complex waters was clearly demonstrated. Now, a validation of the theoretical results presented here needs to be rigorously performed using measurements. The POLDER satellite sensor [*Deschamps et al.*, 1994] was the first one to measure the angular distribution of the polarized radiation from space. Currently, only a few instruments are available to measure the polarized signal, namely the PARASOL satellite sensor, the POLRADS instrument [*Souaidia and Voss*, 2006] and the Research Scanning Polarimeter [*Cairns et al.*, 1999]. The PARASOL sensor, which has a similar design as the POLDER instrument, is a CCD (i.e., Coupled Charge Device) camera with a wide field of view. On this basis, the sensor can observe a ground pixel for several zenith angles (typically 15) thus providing a sample of the bi-directional reflectance distribution function of the observed pixel. The POLRADS instrument is a fish-eye sensor that measures the complete distribution (with respect to azimuth and zenith) of the polarized signal just below the sea surface. The Research Scanning Polarimeter is an airborne instrument that was designed to provide high precision, multiangle measurements of polarization and intensity in a wide spectral range from the visible to shortwave infrared. Even though the analysis of the existing data is currently in progress, great efforts should still be devoted on the development of in-situ polarized instrumentation to significantly increase our knowledge on the optical properties of particles in coastal waters.

Notation

a_{ph}	absorption coefficient of phytoplankton (m^{-1}).
a_{CDOM}	absorption coefficient of colored dissolved organic matter (m^{-1}).
b_{ph}	scattering coefficient of phytoplankton (m^{-1}).
b_{bph}	backscattering coefficient of phytoplankton (m^{-1}).
b_{sed}	scattering coefficient of sediment (m^{-1}).
b_{bsed}	backscattering coefficient of sediment (m^{-1}).
E_d	downwelling irradiance (W m^{-2}).
I, Q, U, V	Stokes vector components (see section 2).
I_p	polarized intensity (W m^{-2} sr^{-1}).
I_s	scattered Stokes vector.
I_v	Stokes vector.
L_u	upwelling radiance (W m^{-2} sr^{-1}).
λ	wavelength (nm).
M	scattering matrix.
0^-	beneath the sea surface.
0^+	above the sea surface.
P	degree of polarization.
$P_{\max}$	maximum value of the degree of polarization.
θ	scattering angle (degree).
θ_s	solar zenith angle (degree).
θ_v	viewing angle (degree).
R	rotation matrix.
ρ	bi-directional reflectance (sr^{-1}).
ρ_{pol}	bi-directional polarized reflectance (sr^{-1}).
τ_a	aerosol optical depth.
AD	Absolute difference (see equation (10)).
CDOM	Colored Dissolved Organic Matter.
Chl	Chlorophyll concentration (mg m^{-3}).
CNES	Centre National d'Etudes Spatiales.
IOCCG	International Ocean Color Coordinating Group.
IOP	Inherent Optical Properties.
OSOA	Ordres Sucessifs Ocean Atmosphere.
PARASOL	Polarization and Anistropy of Reflectances for Atmopsheric Sciences Coupled with Observations from a Lidar.

POLDER POLarization and Directionality of Earth Reflectance.

POLRADS Polarized RAdiance Distribution camera System.

RRMS relative root mean square error $RRMS = \sqrt{\frac{1}{n}\sum_{i=1}^{n}\left(\frac{sed_{i\,\text{estimated}} - sed_{idesired}}{sed_{idesired}}\right)^2}$, where n is the number of measurements and sed_i is the sediment concentration.

RD Relative difference (defined as the absolute difference AD divided by the polarized reflectance ρ_{pol}).

SPM Suspended Particulate Matter.

sed Sediment concentration (mg l^{-1}).

TOA Top of Atmosphere.

[29] **Acknowledgments.** I would like to thank the reviewers for their relevant comments and suggestions.

References

Antoine, D., and A. Morel (1999), A multiple scattering algorithm for atmospheric correction of remotely sensed ocean colour (MERIS instrument): Principle and implementation for atmospheres carrying various aerosols including abosribing ones, *Int. J. Remote Sens.*, *20*, 1875–1916.

Antoine, D., J. M. André, and A. Morel (1996), Oceanic primary production: 2. Estimation at global scale from satellite (Coastal Zone Color Scanner) chlorophyll, *Global Biogeochem. Cycles*, *10*, 57–69.

Babin, M., D. Stramski, G. M. Ferrari, H. Claustre, A. Bricaud, G. Obolensky, and N. Hoepffner (2003), Variations in the light absorption coefficients of phytoplankton, nonalgal particles, and dissolved organic matter in coastal waters around Europe, *J. Geophys. Res.*, *108*(C7), 3211, doi:10.1029/2001JC000882.

Bader, H. (1970), The hyperbolic distribution of particles sizes, *J. Geophys. Res.*, *75*, 2822–2830.

Beardsley, G. F. (1968), Mueller scattering matrix of sea water, *J. Opt. Soc. Am.*, *58*, 52–57.

Boss, E., and W. S. Pegau (2001), Relationship of light scattering at an angle in the backward direction to the backscattering coefficient, *Appl. Opt.*, *40*, 5503–5507.

Bricaud, A., A. Morel, and L. Prieur (1981), Absorption by dissolved organic matter of the sea (yellow substance) in the UV and visible domains, *Limnol. Oceanogr.*, *26*(1), 43.

Bricaud, A., A. Morel, M. Babin, K. Allali, and H. Claustre (1998), Variations of light absorption by suspended particles with chlorophyll *a* concentration in oceanic (case 1) waters: Analysis and implications for bio-optical models, *J. Geophys. Res.*, *103*(C13), 31,033–31,044.

Cairns, B., L. D. Travis, and E. E. Russell (1999), The Research Scanning Polarimeter: Calibration and ground based measurements, in *Polarization, Measurements, Analysis, and Remote Sensing II*, edited by D. H. Goldstein and D. B. Chenault, *Proc. SPIE, 3754*, 186–196.

Carder, K. L., G. F. Beardsley, and H. Pak (1971), Particle size distribution in the eastern equatorial Pacific, *J. Geophys. Res.*, *76*, 5070–5077.

Chami, M., and D. Robilliard (2002), Inversion of oceanic constituents in case I and II waters with genetic programming algorithms, *Appl. Opt.*, *41*(30), 6260–6274.

Chami, M., R. Santer, and E. Dilligeard (2001), Radiative transfer model for the computation of radiance and polarization in an ocean-atmopshere system: polarization properties of suspended matter for remote sensing, *Appl. Opt.*, *40*(15), 2398–2416.

Chowdhary, J., B. Cairns, and L. D. Travis (2002), Case studies of aerosol retrievals over the ocean from multiangle, multispectral photopolarimetric remote sensing data, *J. Atmos. Sci.*, *59*, 383–397.

Chowdhary, J., B. Cairns, and L. D. Travis (2006), Contribution of water leaving radiances to multiangle, multispectral polarimetric observations over the open ocean: Bio-optical model results for case 1 waters, *Appl. Opt.*, *45*(22), 5542–5567.

Deschamps, P. Y., F. M. Bréon, M. Leroy, A. Podaire, A. Bricaud, J. C. Buriez, and G. Sèze (1994), The POLDER mission: Instrument characteristics and scientific objectives, *IEEE Trans. Geosci. Remote Sens.*, *32*(3), 598–615.

Doxaran, D., J. M. Froidefond, and P. Castaing (2002), A reflectance band ratio used to estimate suspended matter concentrations in coastal sediment-dominated waters, *Int. J. Remote Sens.*, *23*, 5079–5085.

Fougnie, B., R. Frouin, P. Lecomte, and P. Y. Deschamps (1999), Reduction of skylight reflections effects in the above water measurement of diffuse marine reflectance, *Appl. Opt.*, *38*(18), 3844–3856.

Goloub, P., D. Tanré, J. L. Deuzé, M. Herman, A. Marchand, and F. M. Bréon (1999), Validation of the first algorithm applied for deriving aerosol properties over the ocean using the POLDER/ADEOS measurements, *IEEE Trans. Geosci. Remote Sens.*, *37*, 1586–1596.

IOCCG (1998), Minimum requirements for an operational ocean colour sensor for the open ocean, *Rep. Int. Ocean Colour Coord. Group*, *1*.

Ivanoff, A., and T. H. Waterman (1958), Factors, mainly depth and wavelength, affecting the degree of underwater light polarization, *J. Mar. Res.*, *16*, 283–307.

Kattawar, G. W., G. N. Plass, and S. J. Hitzfelder (1976), Multiple scattered radiation emerging from Rayleigh and continental haze layer. 1: Radiance, polarization and neutral points, *Appl. Opt.*, *15*, 632–647.

Li, Z., P. Goloub, C. Devaux, X. Gu, J. L. Deuzé, Y. Qiao, and F. Zhao (2006), Retrieval of aerosol optical and physical properties from ground based spectral, multi-angular, and polarized sun-photometer measurements, *Remote Sens. Environ.*, *101*, 519–533.

Loisel, H., and A. Morel (1998), Light scattering and chlorophyll concentration in case 1 waters: A reexamination, *Limnol. Oceanogr.*, *43*, 847–858.

Lundgren, B., and N. K. Hojerslev (1971), Daylight measurements in the Sargasso Sea: Results from the "DANA" expedition January–April 1966, *Rep. 14,* Dep. of Phys. Oceanogr., Univ. of Copenhagen, Copenhagen, Denmark.

Moore, G. F., J. Aiken, and S. Lavender (1999), The atmospheric correction of water color and the quantitative retrieval of suspended particulate matter in case II waters: Application to MERIS, *Int. J. Remote Sens.*, *20*(9), 1713–1733.

O'Reilly, J. E., S. Maritorena, B. G. Mitchell, D. A. Siegel, K. L. Carder, S. A. Garver, M. Kahru, and C. McClain (1998), Ocean color algorithms for SeaWiFS, *J. Geophys. Res.*, *103*, 24,937–24,953.

Plass, G. N., G. K. Kattwar, and S. J. Hitzfelder (1976), Multiple scattered radiation emerging from Rayleigh and continental haze layer. 2: Ellipticity and direction of polarization, *Appl. Opt.*, *15*, 1003–1011.

Pope, R. M., and E. S. Fry (1997), Absorption spectrum (380–700 nm) of pure water. II. Integrating measurements, *Appl. Opt.*, *36*(33), 8710–8723.

Ruddick, K. G., V. De Cauwer, J. Y. Park, and G. Moore (2006), Seaborne measurements of near-infrared water leaving reflectance: The similarity spectrum for turbid waters, *Limnol. Oceanogr.*, *51*(2), 1167–1179.

Souaidia, N., and K. J. Voss (2006), POLRADS: Polarization upwelling radiance distribution measurements, paper presented at Ocean Optics Conference XVIII, Montreal, Canada, 9–13 Oct.

Tassan, S. (1994), Local algorithm using SeaWiFS data for the retrieval of phytoplankton pigments, suspended matter, and yellow substance in coastal waters, *Appl. Opt.*, *33*, 2369–2378.

Van de Hulst, H. C. (1981), *Light Scattering by Small Particles*, 470 pp., Dover, Mineola, N. Y.

Volten, H., J. F. De Haan, J. W. Hovenier, R. Schreurs, W. Vassen, A. G. Dekker, H. J. Hoogenboom, F. Charlton, and R. Wouts (1998), Laboratory measurements of angular distributions of light scattered by phytoplankton and silt, *Limnol. Oceanogr.*, *43*(6), 1180–1197.

Voss, K. J., and E. S. Fry (1984), Measurement of the Mueller matrix for ocean water, *Appl. Opt.*, *23*(23), 4427–4439.

Waterman, T. H. (1954), Polarization patterns in submarine illumination, *Science*, *120*, 927–932.

Waterman, T. H. (1955), Polarization of scattered sunlight in deep waters, *Deep Sea Res.*, *3*, suppl., 426–434.

M. Chami, Université Pierre et Marie Curie-Paris 6, Laboratoire Océanographie de Villefranche, CNRS, 06230 Villefranche sur Mer, France. (chami@obs-vlfr.fr)